Hindawi Publishing Corporation
Journal of Nanomaterials
Volume 2015, Article ID 190747, 9 pages
http://dx.doi.org/10.1155/2015/190747

Research Article

Surfactant-Free Microwave-Assisted Synthesis of Fe-Doped ZnO Nanostars as Photocatalyst for Degradation of Tropaeolin O in Water under Visible Light

Tsz-Lung Kwong and Ka-Fu Yung

Department of Applied Biology and Chemical Technology, The Hong Kong Polytechnic University, Hung Hom, Kowloon, Hong Kong

Correspondence should be addressed to Ka-Fu Yung; bckfyung@polyu.edu.hk

Received 19 March 2015; Accepted 29 June 2015

Academic Editor: Magnus Willander

Iron-doped zinc oxide nanostar was synthesized by the microwave-assisted surfactant-free hydrolysis method. The as-synthesized Fe-doped ZnO nanostars catalyst was fully characterized by scanning electron microscope (SEM), transmission electron microscopy (TEM), energy dispersive X-ray spectroscopy (EDX), powder X-ray diffraction (XRD), and diffuse reflectance UV-vis spectroscopy (UV-DRA). The photocatalytic activity of the photocatalyst was investigated for the photocatalytic degradation of Tropaeolin O under visible light irradiation. It is observed that the doping of Fe ions enhances the absorption of the visible light and thus the photocatalytic degradation rate of Tropaeolin O would increase. Despite the Taguchi orthogonal experimental design method, the photocatalytic conversion could be achieved at 99.8% in the Fe-doped ZnO catalyzed photodegradation reaction under the optimal reaction conditions of catalyst loading (30 mg), temperature (60°C), light distance (0 cm), initial pH (pH = 9), and irradiation time (3 h). The Fe-doped ZnO photocatalyst can also be easily recovered and directly reused for eight cycles with over 70% conversion.

1. Introduction

In the well-developed centuries, textile, paper, and other industries continuously discharge wastewater contaminated with organic dye, definitely harmful to human life and aquatic system. In the recent years, nanostructured metal oxide semiconductor materials played an important role in degradation of organic dyes to maintain an environmental sustainability [1–5]. Zinc oxide (ZnO) is considered as a promising semiconductor compared to titanium dioxide (TiO_2) because of the similar band gap at 3.37 eV, lower cost, and larger exciton binding energy of 60 mV at room temperature [6–8]. However, there are some limitations due to the lower solar utilization and higher charge carrier recombination rate. Some metal nanoparticles such as gold (Au) [9], platinum (Pt) [10], and silver (Ag) [11] were supported on ZnO to enhance the photocatalytic activity on the degradation of organic dye. However, these supported ZnO photocatalysts were only excited by UV light with a limited wavelength shorter than 350 nm. In order to increase the solar utilization and expand the light absorption wavelength to visible light region, some literatures investigated the modification of semiconductors by an incorporation of transition metal (Mn, Cu, Ni, or Co) as dopant into ZnO [12–16]. It is understandable that the introduction of the dopant would narrow the band gap since the delocalized d-energy level insert in between the conduction band and the valence band in which less energy (i.e., longer wavelength) is required to generate a hole [17–20]. Furthermore, semiconductors would greatly inhibit the recombination of photoinduced charge carrier (electron-hole pair) and thus enhance the photocatalytic activity [18, 21].

Various synthetic protocols for synthesis of different nanostructures of ZnO and Fe-doped ZnO have been widely reported by literature including direct calcination of metal salt [21], hydrothermal synthesis [22], sol-gel method [23], and simply hydrolysis followed by calcination [24]. Among all synthetic methods, hydrothermal synthesis is relatively simple and operates under a relatively low temperature.

However, it takes a relatively long reaction time. Microwave irradiation is widely used as heating source which provides a fast and simple synthetic route to heat up the reaction system homogeneously.

In this present study, we reported the synthesis of iron-(Fe-) doped ZnO nanostars by a surfactant-free microwave-assisted hydrolysis towards the photocatalytic degradation of Tropaeolin O under visible light. The as-synthesized Fe-doped ZnO nanostars were fully characterized by SEM, TEM, EDX, XRD, and UV-DRA. Meanwhile, the optimal photocatalytic conditions for degradation of Tropaeolin O under visible light catalyzed by Fe-doped ZnO were determined by Taguchi analysis which has not been reported so far. Stepwise approach has been extensively used; however, it is relatively time consuming and difficult to estimate the optimized conditions as some of the reaction conditions simultaneously affect the photocatalytic degradation. Taguchi analysis is a powerful, cost effective, and relatively time saving optimization approach which consists of orthogonal array experimental design and range analysis [25–28]. The relationship between photocatalytic activity and the reaction conditions including catalyst loading, temperature, light distance, initial pH, and irradiation time was being evaluated in this present study. The photocatalytic durability of the Fe-doped ZnO nanostars catalyst was also examined.

2. Materials and Methods

2.1. Materials. Zinc acetate dihydrate ($Zn(CH_3COO)_2{\cdot}2H_2O$, >98%) was purchased in laboratory reagent grade from BDH Chemical Ltd. Iron(III) nitrate nonahydrate ($Fe(NO_3)_3{\cdot}9H_2O$, purity >99%) was supplied by Acros. Aqueous ammonia solution (NH_4OH, 28.0 wt.%–30.0 wt.%) was purchased from UNI-CHEM. Tropaeolin O was purchased from Sigma Aldrich. The visible light source from the compact fluorescent lamp (65 W) was purchased from local store in Hong Kong.

2.2. Catalyst Preparation and Characterization

2.2.1. Catalyst Preparation. Fe-doped ZnO nanostars catalyst was synthesized by a surfactant-free microwave-assisted hydrolysis without any thermal calcination treatment. Similar synthetic protocol has been reported by Han and coworkers [22] with some modifications. Zinc acetate dihydrate (330 mg) and iron(III) nitrate nonahydrate (3.6 mg) were completely dissolved in milli-Q water (150 mL) to form a transparent mixed metal solution followed by adding aqueous ammonia water (0.16 M). The solution was then heated using a microwave synthesis system (Micro SYNTH) at a fixed temperature of 80°C with a constant microwave power of 400 W for 30 minutes. The precipitate was then washed by milli-Q water and ethanol three times and finally dried at 80°C.

2.2.2. Catalyst Characterization. The size and morphology of the photocatalyst were characterized using a Hitachi S-4800 field emission scanning electron microscope (SEM) which operated at 5 eV and was equipped with energy dispersive spectrometry (EDX) with Horiba EMAX EDS detectors. A JEOL Model JEM-2100F field emission transmission electron microscope (STEM) operated at 200 eV was also used to characterize the photocatalyst. Powder X-ray diffraction (XRD) pattern was collected using a Rigaku SmartLab X-ray Diffractometer equipped with CuKα (λ = 1.54056, 45 kV, 200 mA) radiation with 2θ ranging from 10° to 90° with a step size of 0.02°. The optical absorption spectrum was obtained by Varian Cary 4000 UV-vis spectrophotometer in diffuse reflectance mode.

2.3. Photocatalytic Activity Study. Tropaeolin O was employed as a model of organic dye for the evaluation of the photocatalytic activity of the as-synthesized Fe-doped ZnO nanostars catalyst. For each experimental run, the Fe-doped ZnO nanostars catalyst was suspended in aqueous Tropaeolin O solution (20 mL, 10 mg L^{-1}) with constant vigorous stirring. The photocatalytic reaction was conducted at predesigned temperature under visible light using the compact fluorescent lamp. The photocatalytic decomposition of Tropaeolin O was monitored by measuring the absorbance of the filtered solution at a wavelength of 430 nm using UV-vis spectrophotometer in liquid cuvette configuration with milli-Q water as reference. The photocatalytic conversion (P) of Tropaeolin O can be calculated according to

$$\text{Conversion } (P) = \frac{P_0 - P_t}{P_0} \times 100\%, \quad (1)$$

where P_0 is the initial concentration of Tropaeolin O solution and P_t is the concentration of Tropaeolin O solution at time t.

2.4. Taguchi Analysis for the Fe-Doped ZnO Catalyzed Photocatalytic Degradation of Tropaeolin O. In this photocatalytic study, the optimal reaction conditions for the photocatalytic degradation of Tropaeolin O were designed according to the orthogonal array experimental design and the results were evaluated through the range analysis. Five main processing factors including the catalyst loading (factor A), temperature (factor B), light distance (factor C), initial pH (factor D), and irradiation time (factor E) were designed in four different levels individually as displayed in Table 1.

According to the OA_{16} experimental design, OA_{16} matrix model contains five factors with four levels as distributed in Table 2. In principle, each column of the matrix represents a factor affecting the photocatalytic degradation while each row indicates one experimental run in a combination of specific factors at different level.

The mean K ($\overline{K_{ji}}$) values for the factor j ($j = A, B, C, D$, and E) at level i ($i = 1, 2, 3$, and 4) were simply calculated using the photocatalytic conversions (P) of Tropaeolin O. The level of each factor that gave the highest $\overline{K_{ji}}$ demonstrates that particular level is classified as the optimal level which has a greater influence on the photocatalytic degradation of

Table 1: Factors and levels in the optimization of the photocatalytic degradation of Tropaeolin O through Taguchi analysis.

Level	Factor				
	Catalyst loading A (mg)	Temperature B (°C)	Light distance C (cm)	Initial pH D	Irradiation time E (h)
1	7.5	30	0	5	1.5
2	15.0	40	5	7	2.0
3	22.5	50	10	9	2.5
4	30.0	60	15	11	3.0

Table 2: Orthogonal array experimental design (OA_{16} matrix) for photocatalytic degradation.

Entry	Factor				
	Catalyst loading A (mg)	Temperature B (°C)	Light distance C (cm)	Initial pH D	Irradiation time E (h)
1	1	1	1	1	1
2	1	2	2	2	2
3	1	3	3	3	3
4	1	4	4	4	4
5	2	1	2	3	4
6	2	2	1	4	3
7	2	3	4	1	2
8	2	4	3	2	1
9	3	1	3	4	2
10	3	2	4	3	1
11	3	3	1	2	4
12	3	4	2	1	3
13	4	1	4	2	3
14	4	2	3	1	4
15	4	3	2	4	1
16	4	4	1	3	2

Tropaeolin O. The $\overline{K_{ji}}$ value at different levels for each factor can be calculated as follows:

$$
\begin{aligned}
K_{A1} &= P_1 + P_2 + P_3 + P_4,\\
K_{B1} &= P_1 + P_5 + P_9 + P_{13},\\
K_{C1} &= P_1 + P_6 + P_{11} + P_{16},\\
K_{D1} &= P_1 + P_7 + P_{12} + P_{14},\\
K_{E1} &= P_1 + P_8 + P_{10} + P_{15},\\
\overline{K_{A1}} &= \frac{K_{A1}}{4};\\
\overline{K_{B1}} &= \frac{K_{B1}}{4};\\
\overline{K_{C1}} &= \frac{K_{C1}}{4};\\
\overline{K_{D1}} &= \frac{K_{D1}}{4},\\
\overline{K_{E1}} &= \frac{K_{E1}}{4}.
\end{aligned}
\tag{2}
$$

Furthermore, the largest range value of the factor indicates that the particular factor is the most significant towards the photocatalytic degradation. It is simply calculated by the difference between maximum and minimum $\overline{K_{ji}}$ value according to

$$
\text{Range value} = \max\left(\overline{K_{Ai}}\right) - \min\left(\overline{K_{Ai}}\right), \tag{3}
$$

where $\overline{K_{Ai}}$ is the mean K value of i level ($i = 1, 2, 3$, and 4) of factor A.

3. Results and Discussion

3.1. Characterization of Fe-Doped ZnO Nanostars Photocatalyst. The SEM micrograph as displayed in Figure 1 shows that the as-synthesized Fe-doped ZnO photocatalyst exhibits a star-like morphology with the average particular size of 432.5 ± 5.6 nm. The elemental analysis conducted by EDX shows that the atomic Zn-to-Fe ratio is found to be 99.56 : 0.44. TEM analysis (Figure 2(a)) confirms that the Fe-doped ZnO photocatalyst is exhibiting a star-like morphology with the average size of 300.5 nm. As depicted in HR-TEM (Figure 2(b)), it shows that the pedant arm of the individual nanostar reveals the signal crystalline nature. The crystalline nature of the pedant arm can be derived from SAED. The crystal planes with d-spacing of 0.15 nm, 0.19 nm, and 0.25 nm are attributed to [103], [102], and [101] crystal plane of ZnO in hexagonal phase.

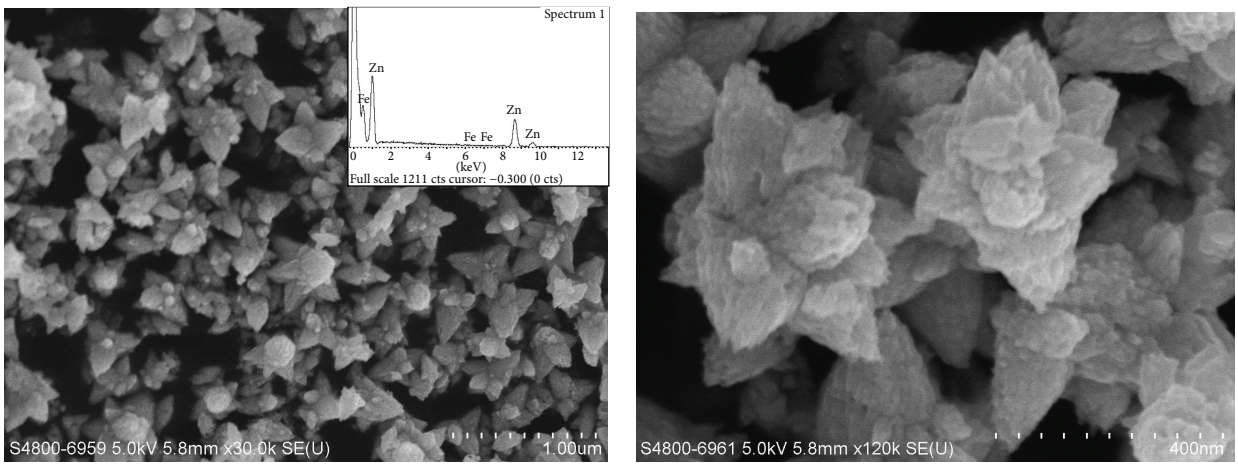

(a) (b)

Figure 1: (a) Low magnification SEM micrograph (insert: EDX spectrum) and (b) high magnification SEM micrograph of the Fe-doped ZnO nanostars photocatalyst.

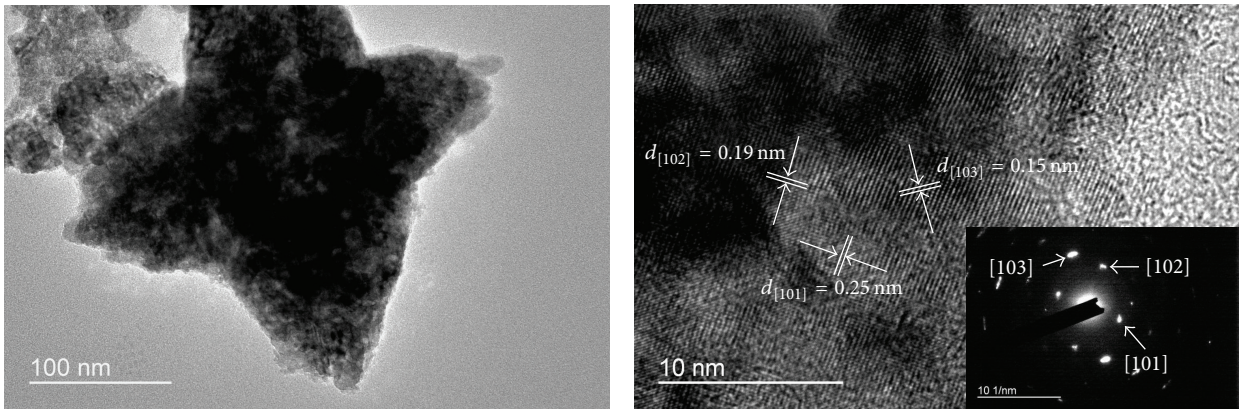

(a) (b)

Figure 2: (a) TEM micrograph of the Fe-doped ZnO nanostar photocatalyst and (b) HR-TEM micrograph of the pedant arm of the Fe-doped ZnO nanostar (insert: SAED micrograph).

The Fe-doped ZnO nanostars photocatalyst was characterized by XRD as shown in Figure 3. The XRD pattern for Fe-doped ZnO photocatalyst exhibits a high degree of crystallinity and matches well with the standard pattern of hexagonal phased zinc oxide with space group P63mc (ICDD card number 00-036-1451). The valence oxidation state of the Fe ions present is proposed to be +3 since iron(III) nitrate was used as precursor and Fe(III) is the most stable oxidation state. As suggested by EDX and XRD analysis, it is confirmed that Fe(III) ions are successfully doped into ZnO lattice without altering the original crystal structure of ZnO. The average crystalline size is found to be 12.7 nm. The lattice constants for the Fe-doped ZnO photocatalyst are found to be a = 3.25 Å, b = 3.25 Å, and c = 5.21 Å.

Figure 4 shows the UV-vis diffuse reflectance spectra of the Fe-doped ZnO and undoped ZnO. The introduction of Fe ions into ZnO crystal lattice exhibits a decrease of the reflectance in the visible region which indicates that the Fe ions doping may enhance the absorption of visible light and thus the Fe-doped ZnO photocatalyst is suitable for an effective photocatalytic degradation of dye under visible light irradiation.

3.2. Taguchi Analysis for the Fe-Doped ZnO Catalyzed Photocatalytic Degradation of Tropaeolin O. Sixteen different experimental runs were carried out according to OA_{16} matrix. The result as tabulated in Table 3 shows the photocatalytic degradation of Tropaeolin O for each experimental run. The conversion ranged from 24.2% to 99.1%. These data are taken as the original data and used in calculation of $\overline{K_{ji}}$ values. The highest $\overline{K_{ji}}$ value for each factor is assigned as the optimal level of reaction condition for the photocatalytic degradation of Tropaeolin O. The highest $\overline{K_{ji}}$ value for each factor as shown in Table 4 is obvious defined in a combination of $A_4B_4C_1D_3E_4$ as the catalyst loading is 30.0 mg (62.1), temperature is 60°C (56.6), light distance is 0 cm (78.0), initial pH

Table 3: A summary of photocatalytic conversion of Tropaeolin O in OA_{16} matrix through Taguchi analysis.

Entry	Factor					Conversion P (%)
	Catalyst loading A (mg)	Temperature B (°C)	Light distance C (cm)	Initial pH D	Irradiation time E (h)	
1	7.5	30	0	5	1.5	29.9
2	7.5	40	5	7	2.0	28.6
3	7.5	50	10	9	2.5	24.9
4	7.5	60	15	11	3.0	25.2
5	15.0	30	5	9	3.0	56.9
6	15.0	40	0	11	2.5	85.3
7	15.0	50	15	5	2.0	24.2
8	15.0	60	10	7	1.5	32.6
9	22.5	30	10	11	2.0	28.7
10	22.5	40	15	9	1.5	36.0
11	22.5	50	0	7	3.0	99.1
12	22.5	60	5	5	2.5	70.8
13	30.0	30	15	7	2.5	44.2
14	30.0	40	10	5	3.0	61.2
15	30.0	50	5	11	1.5	45.2
16	30.0	60	0	9	2.0	97.8

Table 4: Range analysis result for the photocatalytic degradation of Tropaeolin O.

Value name	Factor				
	Catalyst loading A	Temperature B	Light distance C	Initial pH D	Irradiation time E
K_1	108.6	159.7	312.1	186.1	143.7
K_2	199.0	211.1	201.5	204.5	179.3
K_3	234.6	193.4	147.4	215.6	225.2
K_4	248.4	226.4	129.6	184.4	242.4
$\overline{K_1}$	27.2	39.9	78.0	46.5	35.9
$\overline{K_2}$	49.8	52.8	50.4	51.1	44.8
$\overline{K_3}$	58.7	48.4	36.9	53.9	56.3
$\overline{K_4}$	62.1	56.6	32.4	46.1	60.6
Range value (max–min)	35.0	16.7	45.6	7.8	24.7

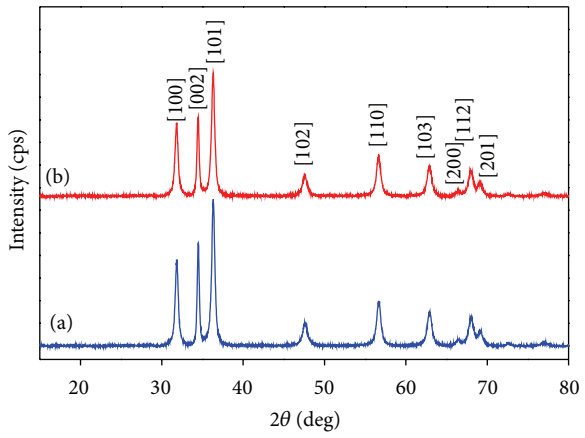

Figure 3: XRD patterns of (a) the undoped ZnO and (b) the Fe-doped ZnO nanostars photocatalyst.

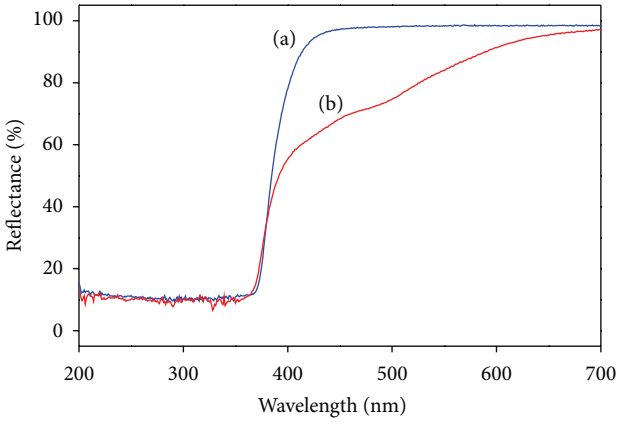

Figure 4: Diffuse UV-vis spectra for (a) the undoped ZnO and (b) the Fe-doped ZnO nanostars photocatalyst.

is 9 (53.9), and the irradiation time is 3.0 h (60.6). The range analysis as shown in Figure 5 demonstrates the significance of each factor in ascending order of initial pH (7.8) > temperature (16.7) > irradiation time (24.7) > catalyst loading (35.0) >

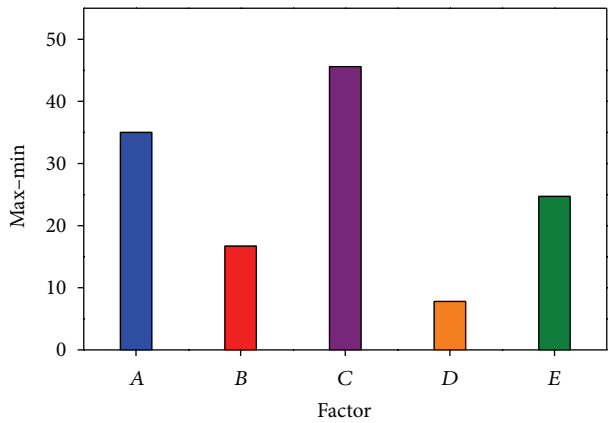

Figure 5: Range values for each factor on the Fe-doped ZnO catalyzed photodegradation of Tropaeolin O.

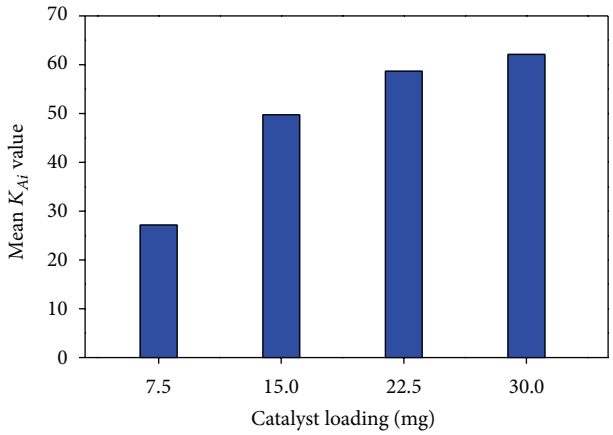

Figure 6: Relationship between catalyst loading and mean K_{Ai} value.

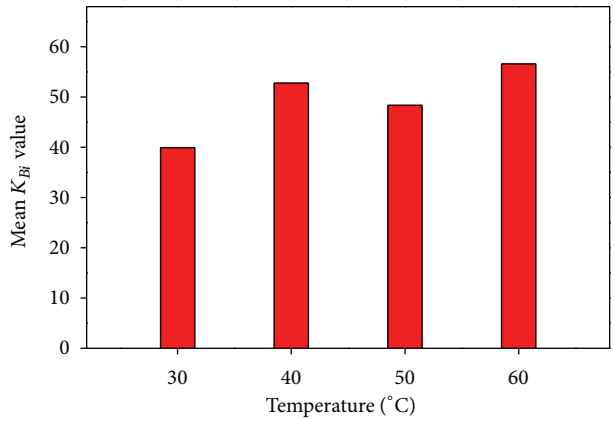

Figure 7: Relationship between temperature and mean K_{Bi} value.

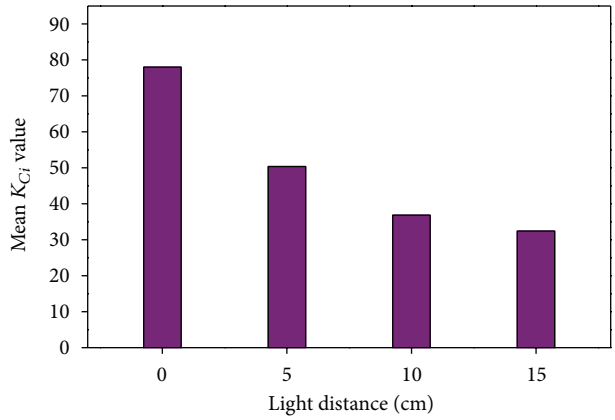

Figure 8: Relationship between light distance and mean K_{Ci} value.

light distance (45.6). The light distance (factor C) gives the largest range value which implies that the photocatalytic degradation changes significantly with slight changing of the distance between visible light source and the reaction flask. A significant change of the initial pH of the aqueous Tropaeolin O solution induces slight changing of the photocatalytic conversion due to the smallest range value obtained.

It is clear from Figure 6 that there is a gradual increase of photocatalytic conversion with the increase of catalyst loading from 7.5 mg to 22.5 mg. It may due to the availably of more active sites on the photocatalyst surface to generate hydroxyl radicals and enhance the photodegradation of the Tropaeolin O. Further increase of catalyst loading to 30 mg did not enhance the photocatalytic conversion significantly as amounts of active sites were already saturated with the limited amount of Tropaeolin O present. The photocatalytic conversion is found to be enhanced with the temperature increased from 30°C to 60°C as observed in Figure 7. The increase in temperature at 60°C would increase the kinetic energy of the Tropaeolin O which leads to a higher diffusion rate and increases the collision between the Tropaeolin O and Fe-doped ZnO nanostars for faster degradation. In contrast, the increase in distance between the visible light source and the reaction flask would decrease the photocatalytic conversion. The highest photocatalytic conversion was observed with zero light distance (Figure 8), since the shortening of the distance provides a higher light intensity for more efficient electron transfer from valence band to conduction band of the photocatalyst. For pH, the highest photocatalytic conversion is obtained at pH 9 (Figure 9). Owing to the amphoteric property of the photocatalyst, the initial pH is an important factor governing the kinetics of photodegradation on the catalyst surface. It affects the surface charge property of the photocatalyst. At higher pH, the present of excess hydroxide (OH^-) facilitates the generation of hydroxyl radicals. However, when the pH was further increased to 11, a significant decrease in activity was observed. At such high pH, dissolution of ZnO is observed which is not favorable for the overall activity. For the reaction time factor, it can be observed that the time required for complete degradation of Tropaeolin O requires at least three hours (Figure 10) in which it is further confirmed in the later confirmative studies.

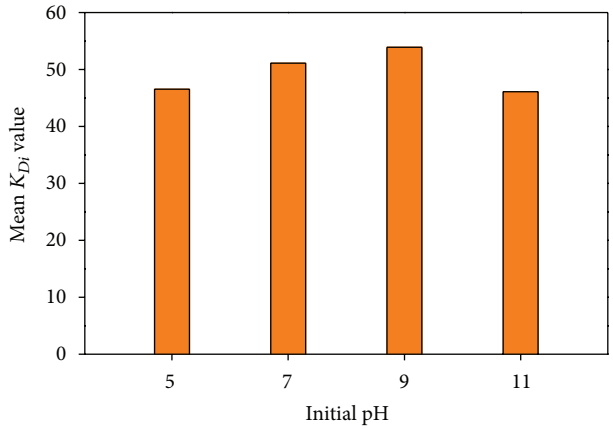

FIGURE 9: Relationship between initial pH and mean K_{Di} value.

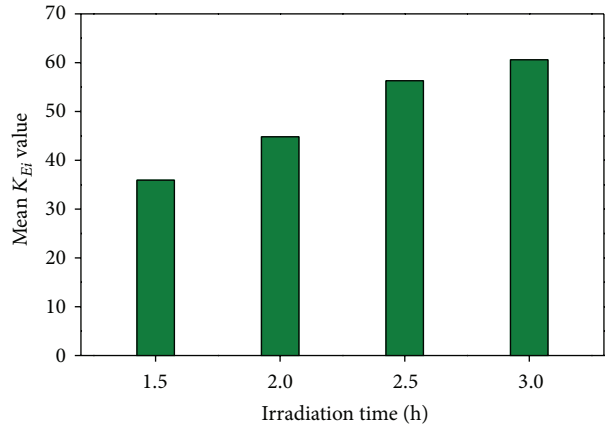

FIGURE 10: Relationship between irradiation time and mean K_{Ei} value.

3.3. Confirmative Experiment. The UV-vis absorption spectra as depicted in Figure 11 record the photocatalytic degradation of Tropaeolin O by Fe-doped ZnO nanostars in a function of time. Tropaeolin O exhibits a maximum adsorption band at wavelength λ_{max} = 430 nm. The absorption peak is gradually decreased and finally disappeared, indicating the Tropaeolin O is degraded with time. As shown in Figure 12, the Fe-doped ZnO catalyzed photodegradation of Tropaeolin O was completed with a conversion of 99.8% under optimized reaction condition for 3 h while a relatively low conversion at 80.0% was obtained for the undoped ZnO catalyst. It indicates that the doping of Fe(III) ions may enhance the absorption of visible light and facilitate the photodegradation of Tropaeolin O. Furthermore, trace amounts of photocatalytic conversion of 2.0% and 4.0% were achieved for the background reaction without any photocatalysts and without visible light irradiation, respectively.

3.4. Photocatalyst Reusability Study. The application of the heterogeneous catalyst towards photocatalytic degradation of dye is beneficial for easier separation. Besides the catalytic activity, the recovery and photocatalytic durability are also

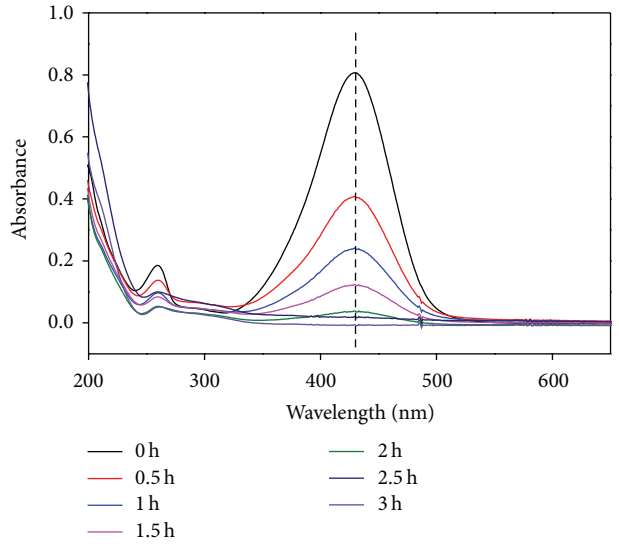

FIGURE 11: UV-vis absorption spectra of Tropaeolin O solution in a function of time. Reaction conditions: catalyst loading (30 mg), temperature (60°C), light distance (0 cm), initial pH (pH = 9), and irradiation time (3 h).

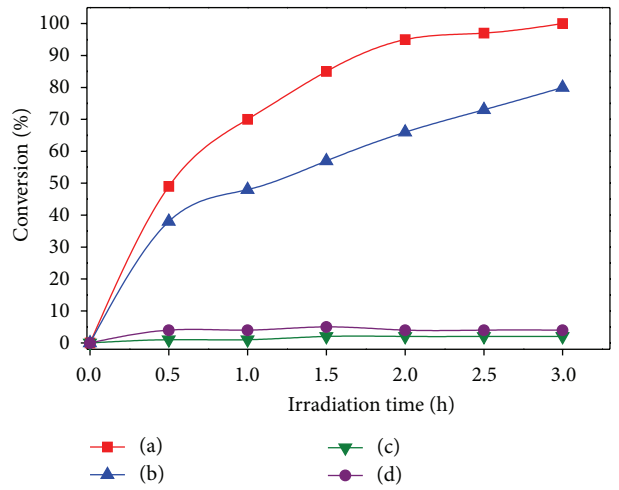

FIGURE 12: The degradation of Tropaeolin O (a) with presence of Fe-doped ZnO nanostars, (b) with presence of undoped ZnO, (c) without any photocatalysts, and (d) without irradiation. Reaction conditions: catalyst loading (30 mg), temperature (60°C), light distance (0 cm), initial pH (pH = 9), and irradiation time (3 h).

one indication to evaluate the catalyst. In this study, a simple approach of direct reuse of photocatalyst without any further washing steps is employed. The reusability study on the Fe-doped ZnO nanostars catalyst for the photocatalytic degradation of Tropaeolin O under optimal conditions was examined. Referring to Figure 13, the Fe-doped ZnO photocatalyst gave 99.8% conversion in the first cycle; however, the conversion gradually decreased to 72.5% at the eighth cycle.

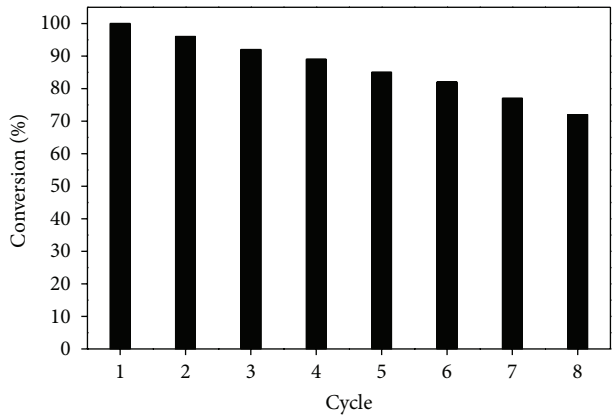

Figure 13: Reusability study on the Fe-doped ZnO nanostar photocatalyst for the degradation of Tropaeolin O under optimal reaction conditions. Reaction conditions: catalyst loading (30 mg), temperature (60°C), light distance (0 cm), initial pH (pH = 9), and irradiation time (3 h).

4. Conclusions

Fe-doped ZnO nanostars photocatalyst was synthesized successfully by the microwave-assisted surfactant-free hydrolysis. The as-synthesized Fe-doped ZnO catalyst was fully characterized by SEM, TEM, EDX, XRD, and UV-DRA. The introduction of Fe ions successfully increases the absorption of visible light and facilitates the photocatalytic degradation of Tropaeolin O. Through the Taguchi analysis and range analysis, the photocatalytic conversion was achieved with 99.8% under optimal reaction conditions of catalyst loading (30 mg), temperature (60°C), light distance (0 cm), initial pH (pH = 9), and irradiation time (3 h). The light distance gave the highest range value which implies that the photocatalytic degradation changes rapidly with changing of the distance between the visible light source and the reaction flask. Furthermore, the Fe-doped ZnO photocatalyst can also be directly reused for six cycles with over 80% conversion.

Conflict of Interests

The authors declare that there is no conflict of interests regarding the publication of this paper.

Acknowledgments

The authors gratefully acknowledge the financial support from Hong Kong Research Grants Council (PolyU5033/13P) and The Hong Kong Polytechnic University. T.-L. Kwong acknowledges the receipt of postgraduate studentship administrated by The Hong Kong Polytechnic University.

References

[1] H. Lachheb, E. Puzenat, A. Houas et al., "Photocatalytic degradation of various types of dyes (Alizarin S, Crocein Orange G, Methyl Red, Congo Red, Methylene Blue) in water by UV-irradiated titania," *Applied Catalysis B: Environmental*, vol. 39, no. 1, pp. 75–90, 2002.

[2] A. Houas, H. Lachheb, M. Ksibi, E. Elaloui, C. Guillard, and J.-M. Herrmann, "Photocatalytic degradation pathway of methylene blue in water," *Applied Catalysis B: Environmental*, vol. 31, no. 2, pp. 145–157, 2001.

[3] S. Dong, K. Xu, and G. Tian, "Photocatalytic activities of $LaFe_{1-x}Zn_xO_3$ nanocrystals prepared by sol-gel auto-combustion method," *Journal of Materials Science*, vol. 44, no. 10, pp. 2548–2552, 2009.

[4] K. Xu and G. Zhu, "Preparation and characterization of nano-La (S, C)-TiO_2 oriented films by template hydrothermal synthesis," *Applied Surface Science*, vol. 255, no. 13-14, pp. 6691–6695, 2009.

[5] Y. Ni, S. Yang, J. Hong, P. Zhen, Y. Zhou, and D. Chu, "Microwave-assisted preparation, characterization and properties of columnar hexagonal-shaped ZnO microcrystals," *Scripta Materialia*, vol. 59, no. 1, pp. 127–130, 2008.

[6] M.-P. Lu, M.-Y. Lu, and L.-J. Chen, "P-type ZnO nanowires: from synthesis to nanoenergy," *Nano Energy*, vol. 1, no. 2, pp. 247–258, 2012.

[7] H. Chen, X. Wu, L. Gong, C. Ye, F. Qu, and G. Shen, "Hydrothermally grown ZnO micro/nanotube arrays and their properties," *Nanoscale Research Letters*, vol. 5, no. 3, pp. 570–575, 2010.

[8] S. Cho, S.-H. Jung, and K.-H. Lee, "Morphology-controlled growth of ZnO nanostructures using microwave irradiation: from basic to complex structures," *The Journal of Physical Chemistry C*, vol. 112, no. 33, pp. 12769–12776, 2008.

[9] P. Pawinrat, O. Mekasuwandumrong, and J. Panpranot, "Synthesis of Au-ZnO and Pt-ZnO nanocomposites by one-step flame spray pyrolysis and its application for photocatalytic degradation of dyes," *Catalysis Communications*, vol. 10, no. 10, pp. 1380–1385, 2009.

[10] G. Sinha, L. E. Depero, and I. Alessandri, "Recyclable SERS substrates based on Au-Coated ZnO nanorods," *ACS Applied Materials and Interfaces*, vol. 3, no. 7, pp. 2557–2563, 2011.

[11] M. J. Height, S. E. Pratsinis, O. Mekasuwandumrong, and P. Praserthdam, "Ag-ZnO catalysts for UV-photodegradation of methylene blue," *Applied Catalysis B: Environmental*, vol. 63, no. 3-4, pp. 305–312, 2006.

[12] R. Ullah and J. Dutta, "Photocatalytic degradation of organic dyes with manganese-doped ZnO nanoparticles," *Journal of Hazardous Materials*, vol. 156, no. 1–3, pp. 194–200, 2008.

[13] K. G. Kanade, B. B. Kale, J.-O. Baeg et al., "Self-assembled aligned Cu doped ZnO nanoparticles for photocatalytic hydrogen production under visible light irradiation," *Materials Chemistry and Physics*, vol. 102, no. 1, pp. 98–104, 2007.

[14] C. Wu, L. Shen, H. Yu, Y.-C. Zhang, and Q. Huang, "Solvothermal synthesis of Cu-doped ZnO nanowires with visible light-driven photocatalytic activity," *Materials Letters*, vol. 74, pp. 236–238, 2012.

[15] S. V. Bhat and F. L. Deepak, "Tuning the bandgap of ZnO by substitution with Mn^{2+}, Co^{2+} and Ni^{2+}," *Solid State Communications*, vol. 135, no. 6, pp. 345–347, 2005.

[16] M. Anpo and M. Takeuchi, "The design and development of highly reactive titanium oxide photocatalysts operating under visible light irradiation," *Journal of Catalysis*, vol. 216, no. 1-2, pp. 505–516, 2003.

[17] X. Qiu, L. Li, J. Zheng, J. Liu, X. Sun, and G. Li, "Origin of the enhanced photocatalytic activities of semiconductors: a case study of ZnO doped with Mg^{2+}," *Journal of Physical Chemistry C*, vol. 112, no. 32, pp. 12242–12248, 2008.

[18] Y. Cao, T. He, Y. Chen, and Y. Cao, "Fabrication of rutile TiO_2-Sn/Anatase TiO_2-N heterostructure and its application in

visible-light photocatalysis," *The Journal of Physical Chemistry C*, vol. 114, no. 8, pp. 3627–3633, 2010.

[19] H. Irie, Y. Watanabe, and K. Hashimoto, "Nitrogen-concentration dependence on photocatalytic activity of TiO_2-xNx powders," *Journal of Physical Chemistry B*, vol. 107, no. 23, pp. 5483–5486, 2003.

[20] R. Nakamura, T. Tanaka, and Y. Nakato, "Mechanism for visible light responses in anodic photocurrents at N-doped TiO_2 film electrodes," *Journal of Physical Chemistry B*, vol. 108, no. 30, pp. 10617–10620, 2004.

[21] K.-Z. Zhang, B.-Z. Lin, Y.-L. Chen et al., "Fe-doped and ZnO-pillared titanates as visible-light-driven photocatalysts," *Journal of Colloid and Interface Science*, vol. 358, no. 2, pp. 360–368, 2011.

[22] L. Han, D. Wang, Y. Lu et al., "Influence of annealing temperature on the photoelectric gas sensing of Fe-doped ZnO under visible light irradiation," *Sensors and Actuators B: Chemical*, vol. 177, pp. 34–40, 2013.

[23] A. Hernández, L. Maya, E. Sánchez-Mora, and E. M. Sánchez, "Sol-gel synthesis, characterization and photocatalytic activity of mixed oxide ZnO-Fe_2O_3," *Journal of Sol-Gel Science and Technology*, vol. 42, no. 1, pp. 71–78, 2007.

[24] S. Dong, K. Xu, J. Liu, and H. Cui, "Photocatalytic performance of ZnO:Fe array films under sunlight irradiation," *Physica B: Condensed Matter*, vol. 406, no. 19, pp. 3609–3612, 2011.

[25] X. Wu and D. Y. C. Leung, "Optimization of biodiesel production from camelina oil using orthogonal experiment," *Applied Energy*, vol. 88, no. 11, pp. 3615–3624, 2011.

[26] J. Wu and H. K. Lee, "Orthogonal array designs for the optimization of liquid-liquid-liquid microextraction of nonsteroidal anti-inflammatory drugs combined with high-performance liquid chromatography-ultraviolet detection," *Journal of Chromatography A*, vol. 1092, no. 2, pp. 182–190, 2005.

[27] W. G. Lan, M. K. Wong, N. Chen, and Y. M. Sin, "Orthogonal array design as a chemometric method for the optimization of analytical procedures. Part 1. Two-level design and its application in microwave dissolution of biological samples," *The Analyst*, vol. 119, no. 8, pp. 1659–1667, 1994.

[28] W. G. Lan, M. K. Wong, N. Chen, and Y. M. Sin, "Orthogonal array design as a chemometric method for the optimization of analytical procedures. Part 2. Four-level design and its application in microwave dissolution of biological samples," *The Analyst*, vol. 119, no. 8, pp. 1669–1675, 1994.